

# Gamma-ray variability of radio-loud narrow-line Seyfert 1 galaxies

G. Calderone<sup>1\*</sup>, L. Foschini<sup>2</sup>, G. Ghisellini<sup>2</sup>, M. Colpi<sup>1</sup>, L. Maraschi<sup>3</sup>,  
F. Tavecchio<sup>2</sup>, R. Decarli<sup>4</sup>, G. Tagliaferri<sup>2</sup>

<sup>1</sup> *Università di Milano - Bicocca, Dip. di Fisica G. Occhialini, Piazza della Scienza 3, I-20126 Milano, Italy*

<sup>2</sup> *INAF Osservatorio Astronomico di Brera, Via E. Bianchi 46, I-23807 Merate (LC), Italy*

<sup>3</sup> *INAF Osservatorio Astronomico di Brera, Via Brera 28, I-20121 Milano, Italy*

<sup>4</sup> *Max-Planck-Institut für Astronomie, Königstuhl 17, D-69117 Heidelberg, Germany*

Accepted 2011 January 06. Received 2011 January 06; in original form 2010 November 16

## ABSTRACT

The recent detection of  $\gamma$ -ray emission from four radio-loud narrow-line Seyfert 1 galaxies suggests that the engine driving the AGN activity of these objects share some similarities with that of blazars, namely the presence of a  $\gamma$ -ray emitting, variable, jet of plasma closely aligned to the line of sight. In this work we analyze the  $\gamma$ -ray light curves of the four radio-loud narrow-line Seyfert 1 galaxies for which high-energy gamma-ray emission has been discovered by *Fermi*/LAT, in order to study their variability. We find significant flux variability in all the sources. This allows us to exclude a starburst origin of the  $\gamma$ -ray photons and confirms the presence of a relativistic jet. Furthermore we estimate the minimum  $e$ -folding variability timescale (3 – 30 days) and infer an upper limit for the size of the emitting region (0.2 – 2 pc, assuming a relativistic Doppler factor  $\delta = 10$  and a jet aperture of  $\theta = 0.1$  rad).

**Key words:** galaxies: jets – galaxies: Seyfert – galaxies: individual: PMN J0948+0022 – 1H 0323+342 – PKS 1502+036 – PKS 2004-447 – gamma-rays: observations.

## 1 INTRODUCTION

Narrow-line Seyfert 1 (NLS1) galaxies are a class of AGN characterized by a rather narrow width of the  $H\beta$  emission line (FWHM  $\lesssim 2000$  km/s), and by the presence of a strong FeII bump, a soft X-ray excess and flux ratio  $[OIII]/H\beta < 3$  (Osterbrock & Pogge 1985; Pogge 2000). These sources are usually radio-quiet, although, in a few cases, they show a radio-loudness parameter R (ratio between the 5 GHz and optical B flux densities, Kellermann et al. 1989) greater than 1000 (Komossa et al. 2006; Yuan et al. 2008). Such sources, dubbed radio-loud narrow-line Seyfert 1 galaxies (RL-NLS1), were thought to be inactive in  $\gamma$ -rays, although several authors speculated the occurrence of similarities with blazars (Zhou et al. 2003; Komossa et al. 2006; Zhou et al. 2007; Yuan et al. 2008; Foschini et al. 2009; Gu & Chen 2010). The important discovery of  $\gamma$ -ray emission from the RL-NLS1 source PMN J0948+0022 (Foschini et al. 2010b; Abdo et al. 2009a) confirmed these similarities, i.e. the presence of a jet closely aligned to the line of sight as a source of Compton up-scattered  $\gamma$ -ray photons. PMN J0948+0022

( $z=0.585$ , Williams et al. 2002) is one of the strongest radio source among the RL-NLS1; for its fast radio variability, source compactness, inverted radio spectrum and high brightness temperature, PMN J0948+0022 is one of the first RL-NLS1 for which the presence of a jet has been hypothesized (Zhou et al. 2003; Doi et al. 2006). The detection of  $\gamma$ -ray emission definitively confirms the presence of a jet and allows to build a complete SED which closely resemble that of a typical blazar, with two broad peaks in the far IR and in the  $\gamma$ -ray range respectively. By modeling the SED with the synchrotron and inverse-Compton model (Ghisellini & Tavecchio 2009) it is possible to roughly estimate important parameters such as the black hole mass, the Eddington ratio, and the power carried by the jet. The resulting values, although model-dependent, are usually compatible with estimates found independently in other studies. In the case of PMN J0948+0022 the black hole mass turns out to be  $\sim 1.5 \times 10^8 M_{\odot}$  (compatible with the range of values found by Zhou et al. 2003 using the empirical relation between the FWHM of emission lines and the continuum luminosity), and the Eddington ratio which is  $\sim 40\%$ . A  $\gamma$ -ray variability of a factor 2.2 rules out the possibility that the  $\gamma$ -ray emission is due to a starburst contribution (Abdo et al. 2009b). Shortly after this discovery, three

\* E-mail: giorgio.calderone@mib.infn.it

more RL-NLS1 had been observed in  $\gamma$ -rays (Abdo et al. 2009c): 1H 0323+342, PKS 1502+036 and PKS 2004-447, thus confirming that at least some RL-NLS1 are  $\gamma$ -ray emitting AGN. The SED of these sources has also been modeled with the synchrotron and inverse-Compton model, providing black hole mass estimates in agreement with previous studies (see Abdo et al. 2009c, and references therein). 1H 0323+342 ( $z=0.06$ , Marcha et al. 1996) is considered to be a composite nucleus of a NLS1 (for its optical spectrum properties typical of NLS1) and a blazar (for its flat radio spectrum, core compactness and X-rays variability, Zhou et al. 2007). It is the only  $\gamma$ -ray detected RL-NLS1 for which we have an *HST*/WFPC2 optical image of the host galaxy. The host shows a ring-like structure of 15.6 kpc in diameter and the entire galaxy looks like a one-armed spiral (Zhou et al. 2007). Another study, based on NOT data, suggests that 1H 0323+342 may be the remnant of a galaxy merger (Antón et al. 2008). The most striking feature of this source is the high luminosity of the accretion disc which, according to SED modeling, is approximately 90% of Eddington value (Abdo et al. 2009c). PKS 1502+036 ( $z=0.41$ , Snellen et al. 2002) is the second most powerful source in terms of Eddington ratio (80 per cent). It carries a jet power, inferred from SED modeling, slightly lower than PMN J0948+002 (Abdo et al. 2009c). Finally, PKS 2004-447 ( $z=0.24$ , Drinkwater et al. 1997) is an unusual RL-NLS1. It is a strong radio emitter, with the highest radio-loudness parameter ( $R>6000$ ) among the four  $\gamma$ -ray detected RL-NLS1. PKS 2004-447 has an unusually weak Fe II complex compared to other NLS1 and a rather steep (although variable) radio spectral index compared to the other RL-NLS1. Oshlack et al. (2001) suggests that it may be well classified as a low-luminosity compact steep spectrum (CSS) radio quasar, also considering its low inferred black hole mass ( $\sim 10^6 M_{\odot}$ ) (Abdo et al. 2009c). Spectral fit of the SED may require a thermal Comptonization component (Gallo et al. 2006) or an external Compton component (Abdo et al. 2009c).

The detection of  $\gamma$ -rays from the four mentioned RL-NLS1 allows to identify a new class of  $\gamma$ -ray emitting AGN. The radio properties (namely temporal variability, flat spectrum and high brightness temperature) together with the  $\gamma$ -ray detection suggests the presence of a relativistic jet closely aligned to the line of sight. Low power, mildly relativistic and poorly collimated radio jets have already been observed in a few spiral galaxies hosting Seyfert nuclei (e.g. Keel et al. 2006, and references therein), but in the case of PMN J0948+0022 and PKS 1502+036 the power carried by the jet, as inferred from SED modeling, is in the range of quasars, while in 1H 0323+342 and PKS 2004-447 is in the range of BL Lac objects (Abdo et al. 2009c). Such powerful jets are observed only in blazars hosted in elliptical galaxies (Marscher 2009) with black hole masses in the range  $10^8 - 10^9 M_{\odot}$ . By contrast black hole masses in  $\gamma$ -ray detected RL-NLS1 ( $10^6 - 10^8 M_{\odot}$ ) are up to three orders of magnitude smaller than for blazars, thus suggesting that these sources emit at high Eddington ratios. Furthermore, it seems that the  $M_{\text{BH}}-\sigma_*$  scaling relation does not apply to NLS1, mainly due to their small FWHM of permitted lines. Decarli et al. (2008) showed that a reconciliation with the scaling relation is possible if the broad line region is assumed to have a disc-like geometry (but see Marconi et al. 2008).

While the  $\gamma$ -ray variability of PMN J0948+0022 has already been studied in Abdo et al. (2009b) and, with a higher level of significance, during the outburst occurred in July 2010 (Foschini et al. 2010c), it has never been studied for the remaining three sources. Aim of this paper is to analyze the *Fermi*/LAT light curves of the afore-mentioned RL-NLS1 galaxies in order to put the  $\gamma$ -ray variability on a firm basis, and to find the minimum  $\gamma$ -ray variability timescale. Throughout the paper, we assume a  $\Lambda$ CDM cosmology with  $H_0 = 71 \text{ km s}^{-1} \text{ Mpc}^{-1}$ ,  $\Omega_m = 0.27$ ,  $\Omega_{\Lambda} = 0.73$ .

## 2 DATA ANALYSIS

The data analysis has been performed following the standard procedure described in the *Fermi*/LAT documentation. The Science Tools software version is 9.15.2 and the IRF is P6\_V3\_DIFFUSE. Data span the period from 2008 august 4 to 2010 october 08 ( $\sim 26$  months). For each RL-NLS1 all class 3 (diffuse) events coming from a zenith angle  $< 105^\circ$  were extracted within an acceptance cone of radius  $10^\circ$  around the catalog source position. The unbinned likelihood analysis has been performed modeling the spectrum of each RL-NLS1 and of all nearby ( $< 10^\circ$ ) sources present in the LAT 1-year point source catalog (Abdo et al. 2010b) with a power law in the range 0.1 – 100 GeV. We computed the integrated flux for each source analyzing all data over the entire period of 26 months. The extension of the region of interest to  $15^\circ$  around the catalog position results in non-significant variations of the flux, number of counts and TS (Test Statistic, Mattox et al. 1996), as expected since the PSF of LAT is at most  $5^\circ$  wide at 100 MeV. We also performed the same analysis using alternative spectral models. The use of a broken power law instead of a simple power law model yields to a slight increase in the values of TS for PMN J0948+0022 (from 993 to 1194) and 1H 0323+342 (from 86 to 115), and a decrease for PKS 1502+036 and PKS 2004-447. With a log-parabola, the values of TS remain essentially the same as for the case of a power law for PMN J0948+0022 (from 993 to 999) and PKS 2004-447 (from 97.4 to 98.5), while they decrease for 1H 0323+342 and PKS 1502+036. In the following analysis we will therefore use the power law models. Then we extracted light curves with time binning of 15 days (Fig. 1; the time binning for PKS 2004-447 is 30 days) using a TS threshold of 10 (TS>10, roughly equivalent to  $3\sigma$ , Mattox et al. 1996) and performed a chi-squared test against the null hypothesis of constant flux. If the detection was not significant (TS<10) we computed an upper limit to the flux by varying the source flux value (obtained through maximization of likelihood) until TS reaches a value of 4 (Abdo et al. 2010b). The resulting fluxes (denoted with arrows in the figure) corresponds to  $2\sigma$  upper limits. When TS<1 we didn't compute the upper limit since it would be overestimated.

We further proceeded on the analysis of the light curves in order to compute the minimum  $e$ -folding timescale for each source. We extracted light curves with different time binnings starting from 30 days. When the detection is significant (TS>10) we re-run the analysis halving the time bin interval, down to a minimum of approximately 6 hours (roughly corresponding to four *Fermi* orbits, thus ensuring that each source is observed at least twice for each tem-

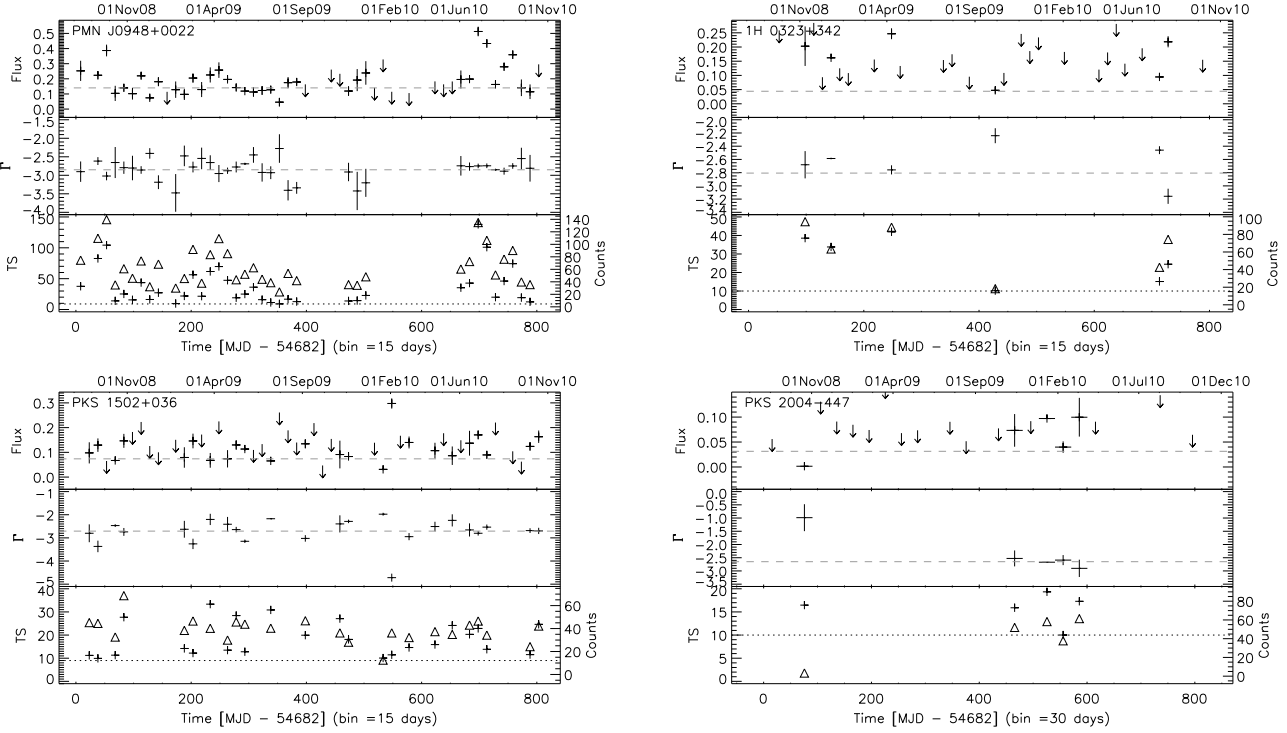


**Figure 1.** Upper panels: light curves of the four RL-NLS1 for detections with  $TS > 10$ . Fluxes are given in units of  $10^{-6}$  ph cm $^{-2}$  s $^{-1}$  in the range 0.1 – 100 GeV. Vertical error bars correspond to  $1\sigma$  errors, while horizontal bars corresponds to the time binning (15 days for PMN J0948+0022, 1H 0323+342 and PKS 1502+036, 30 days for PKS 2004-447). Upper limits ( $TS < 10$ ) at  $2\sigma$  level are denoted by arrows. Middle panels: photon indices. Vertical error bars correspond to  $1\sigma$  errors. In both panels horizontal dashed lines are the integrated (over the entire period of 26 months) flux value and photon index respectively. Lower panels: TS values (plus symbols) and number of counts (triangle symbols, values on the right axis), the horizontal dotted line is the threshold ( $TS = 10$ ).

poral bin). Then, we considered all combinations of non-overlapping time bins with the following characteristics: (1) both time bins have a significant detection,  $TS > 10$ ; (2) the flux difference is greater than the greatest flux error involved at the  $3\sigma$  level; (3) the count difference is significant at the  $3\sigma$  level, assuming a Poisson statistic; (4) the number of counts in each bin must be greater than 3. For such pairs of bins we computed the  $e$ -folding timescale as:

$$\tau_{ij} = \left| \frac{t_i - t_j}{\ln F_i / F_j} \right| \quad (1)$$

where  $i$  and  $j$  are the indices of the involved time bins ( $i > j$ ). The associated error (at  $3\sigma$  level) is computed through error propagation:

$$\Delta\tau_{ij} = \frac{\tau_{ij}}{t_i - t_j} \left[ (\Delta t_{ij})^2 + \left( \tau_{ij} \frac{\Delta F_i}{F_i} \right)^2 + \left( \tau_{ij} \frac{\Delta F_j}{F_j} \right)^2 \right]^{1/2} \quad (2)$$

where  $\Delta t_{ij}$  is half the width of the wider time bin involved,  $\Delta F_i$  and  $\Delta F_j$  are the  $3\sigma$  error on fluxes. We compute the minimum  $e$ -folding variability timescale as  $\tau = \min(\tau_{ij})$ , and associate the corresponding error  $\Delta\tau$  using Eq. 2. The reliability of Eq. 2 has been assessed by simulating 4 series (respectively for  $t_i$ ,  $F_i$ ,  $t_j$  and  $F_j$ ) of 10000 normally distributed values. The resulting values of  $\tau$  are normally distributed and the  $3\sigma$  confidence intervals are correctly estimated by  $\Delta\tau$  when the mean and standard deviation of the simulated data are used in Eq. 2.

### 3 RESULTS

Fig. 1 shows the light curves (upper panels) of the four RL-NLS1 over the entire period of 26 months. Vertical error bars are  $1\sigma$  errors on fluxes, while horizontal bars are equal to the time binning (15 days, except PKS 2004-447 for which is 30 days) for all points with a significant detection ( $TS > 10$ ). Points without a significant detection are upper limits denoted by arrows. Middle panels show the photon indices for points with significant detection, assuming a simple power law model ( $F(E) \propto E^\Gamma$ ) for each source in the range 0.1 – 100 GeV. Horizontal dashed lines in both upper and middle panels are the integrated (over 26 months) flux and photon index respectively. Lower panels show the TS value (plus symbol) and number of counts (triangle symbol) for each bin with significant detection. The integrated luminosity and photon indices, as well as the  $\chi^2$  values and DOF in the hypothesis of constant flux, are reported in Table 1. The minimum  $e$ -folding variability timescale computed with Eq. 1 and 2 is reported in Table 1. The detailed view (zoom) on the time bins involved in the computation of the minimum  $e$ -folding variability timescale are shown in Fig. 2. To compute  $\tau$ , points with different time binnings are considered and are denoted with different horizontal bar lengths in Fig. 2 (e.g. for PMN J0948+0022, one time binning is 0.23 days and the other is 7.5 days. The bar corresponding to the shorter time bin is barely visible). Similarly, vertical bars refer to  $1\sigma$  errors in the flux. The square symbols identify the points that fulfill the constraints described in Sect.

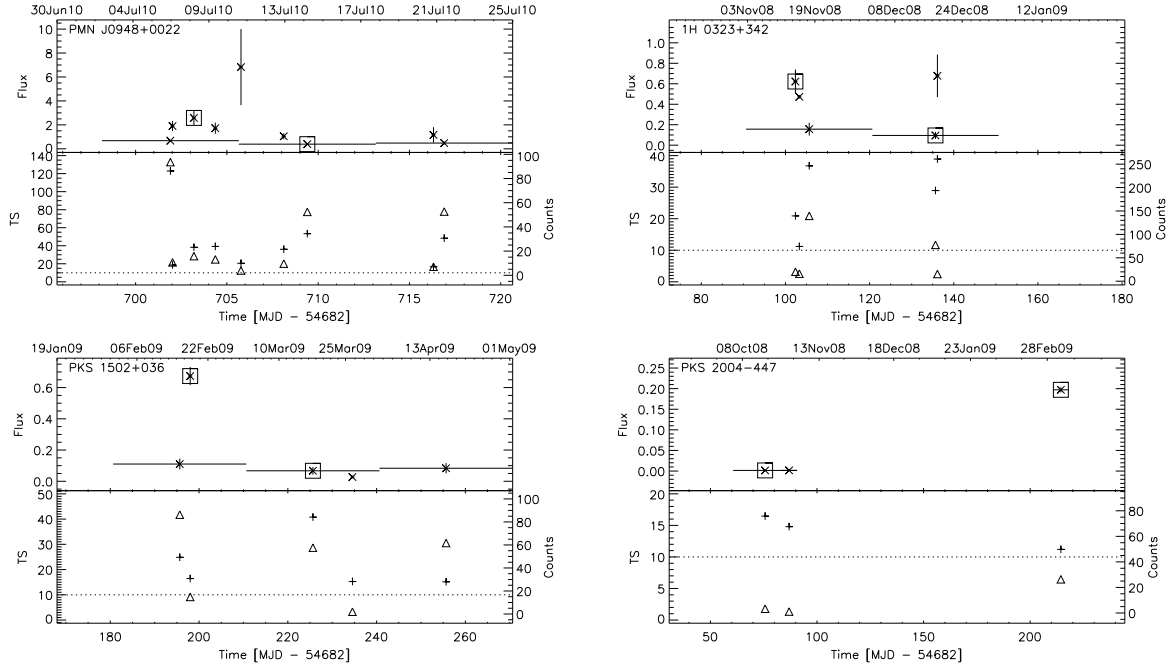


**Figure 2.** Detail view on the bins (denoted by squares) involved in the computation of the  $e$ -folding minimum variability timescale. Units and meaning of symbols are the same as in Fig. 1 (upper and lower panels). Flux symbols have been changed to  $\times$  for a clearer visibility. See also Table 2.

**Table 1.** Data and results of the analysis on the four RL-NLS1 sources. Columns are: (1) name of the source; (2) redshift; (3) luminosity distance; (4) radio loudness; (5) integrated  $\gamma$ -ray luminosity (0.1 – 100 GeV) over the entire period (26 months) with errors at  $1\sigma$  level; (6) photon index with errors at  $1\sigma$  level; (7)  $\chi^2$  and (8) DOF computed on the light curves of Fig. 1 in the null hypothesis of constant flux equal to the integrated flux; (9) minimum  $e$ -folding variability timescale with error at  $3\sigma$  level.

Source	$z$	$D_L$ [Gpc]	R	$L_\gamma$ [ $10^{45}$ erg s $^{-1}$ ]	$\Gamma$	$\chi^2$	DOF	$\tau$ [days]
PMN J0948+0022	0.59	3.40	1000	$250.00 \pm 13.04$	$-2.851 \pm 0.007$	528	33	$3.3 \pm 2.5$
1H 0323+342	0.06	0.27	151	$0.16 \pm 0.04$	$-2.807 \pm 0.010$	2575	5	$17.7 \pm 14.4$
my PKS 1502+036	0.41	2.20	1549	$41.45 \pm 4.10$	$-2.708 \pm 0.007$	385	21	$12.0 \pm 9.0$
PKS 2004-447	0.24	1.20	6320	$3.85 \pm 0.70$	$-2.650 \pm 0.006$	4032	4	$28.4 \pm 18.5$

**Table 2.** Quantities involved in the computation of the minimum  $e$ -folding variability timescale.

Source	$t^a$ [days]	$\Delta t^b$ [days]	$F_\gamma^c$ [ $10^{-6}$ ph cm $^{-2}$ s $^{-1}$ ]	$N / \Delta t$ [cts days $^{-1}$ ]	TS
PMN J0948+0022	703.20	0.23	$2.578 \pm 0.584$	67.5	38
	709.40	7.50	$0.389 \pm 0.058$	7.0	53
1H 0323+342	102.40	0.94	$0.622 \pm 0.117$	21.5	21
	135.70	30.00	$0.095 \pm 0.034$	2.6	29
PKS 1502+036	198.00	0.94	$0.674 \pm 0.058$	15.8	16
	225.70	30.00	$0.067 \pm 0.025$	1.9	41
PKS 2004-447	75.66	30.00	$0.001 \pm 0.001$	0.1	16
	214.40	7.50	$0.197 \pm 0.006$	3.5	11

<sup>a</sup> MJD - 54682

<sup>b</sup> Time binning.

<sup>c</sup> Flux in the range 0.1 – 100 GeV.

2 and provide the value of  $\tau$ . Notice, as an example, that the point at time  $\sim 706$  (MJD - 54682, PMN J0948+0022) is excluded from the computation since its flux value is compatible with nearby points at  $3\sigma$  level (rule (2) of Sect. 2). The quantities involved in the calculation of  $\tau$  (time, time binning, photon flux, number of counts and TS values) are reported in Table 2.

#### 4 DISCUSSION

A statistically significant variability over the entire period of 26 months is present for all sources. The significance of this variability on timescales of  $\lesssim 2$  years is supported by the chi-squared test performed against the null hypothesis of constant flux (last two columns of Table 1). This rules out the possibility that the  $\gamma$ -ray emission is due to a starburst activity. Thus, the data support the hypothesis that  $\gamma$ -ray photons are associated to the presence of a jet. We cannot exclude the possibility of a starburst activity but its contribution would be negligible compared to the jet emission, since the  $\gamma$ -ray luminosities (Table 1) found in our RL-NLS1 are at least four order of magnitude greater than the archetypal starburst galaxy M82 hosting a quiescent black hole (Gaffney et al. 1993) and whose  $\gamma$ -ray luminosity in the 0.1 – 100 GeV range is  $\sim 10^{40}$  erg s $^{-1}$  (Abdo et al. 2010a).

The next step in our analysis has been to estimate the minimum timescale variability for each source. Among the many methods to measure a timescale variability we chose the  $e$ -folding timescale (Eq. 1). The main advantage of this method is that it allows a computation of the timescale using just two flux measurements; it does not require any fitting or minimising procedure. Furthermore the resulting timescale is well defined and can be used to compare different sources. Finally, the error on the timescale is easily computed using analytical error propagation (Eq. 2). The underlying assumption is that the flux evolve according to an (either increasing or decreasing) exponential law. Although this assumption is not always justified (e.g. in the presence of flaring episodes) it is of common practice since we often do not know the actual law which drives the evolution of the flux. Furthermore, the requirement of just two flux measurements can be easily accomplished even for weak sources such as the ones analyzed in this work. The rules to select the flux measurements used in the computation of the  $e$ -folding timescale have been described in Sect. 2: rules (2) and (3) are needed to ensure that the flux in the two temporal bins are actually different, otherwise our assumption of exponentially varying flux cannot be justified. Rules (1) and (4) ensure that the flux measures and associated errors are reliable. The relative error  $\Delta\tau/\tau$  of our measure of the minimum  $e$ -folding timescale depends on several factors. The main sources of uncertainties are the errors in the flux measurements  $\Delta F$  and the width of the time bins  $\Delta t$ . The ratio  $\Delta F/F$  can be made smaller by increasing the number of counts detected in a wider time bin (greater  $\Delta t$ ). Viceversa, a narrower time bin results in a smaller number of counts and consequently a poor accuracy in the flux measurement. The best achievable accuracy on  $\tau$  (that is the smaller value of  $\Delta\tau/\tau$ ) is thus determined by the trade-off between the narrowness of the time bin and the accuracy of flux measurements. Notice however that the narrowness of the time bin is limited by

the requirement that the source is detected with high significance,  $TS > 10$  (rule (1) in Sect. 2). Since the shortest width of the time bins scales linearly with the inverse of the photon flux, we may use narrower time bins (and detect shorter timescales) on brighter sources. The accuracy of  $\tau$  is improved if we compute the  $e$ -folding timescale using non-contiguous time bins, since the exponential law is better constrained by distant points rather than closer ones. On the other hand, if the bins are contiguous, the error  $\Delta\tau$  may be significantly greater than  $\tau$  itself, i.e. the measure would be useless. The issue related to the computation of  $\tau$  with non-contiguous time bins is that we are deliberately ignoring what lies between the two time bins, even if we have a significant measure. An example is given in Fig. 2 for PMN J0948+0022 (upper-left panel) where the minimum  $e$ -folding timescale is computed ignoring the flux measurement at time  $\sim 706$  (MJD - 54682). The reason is that the flux measure has a rather big error bar, which does not allow us to consider it statistically incompatible at the  $3\sigma$  level with neighbouring flux measures (rule (2) in Sect. 2). This example suggests that the intrinsic variability timescale, i.e. a measure of “how fast” the source is able to change its flux significantly, may be shorter than our measure of  $\tau$ , although we cannot assess it on a firm statistical basis. This is a consequence of the fact that we are assuming a particular function (the exponential) and that we are using only two flux measurements instead of all available data. If our detector were able to monitor the flux evolution continuously, we could have employed more sophisticated methods, such as the Fourier analysis, in order to estimate the intrinsic minimum timescale variability. Actually, our light curves do not allow a continuous monitoring of the sources with time binning of 30 days, and we are thus forced to rely on the  $e$ -folding timescale. As a consequence, our measure of  $\tau$  should be considered as an upper limit for the intrinsic minimum timescale variability. The sources display an  $e$ -folding minimum timescale variability in the range of 3 – 30 days. In particular, variability of the order of  $\sim$ days has been found for PMN J0948+0022, and of the order of  $\sim$ tens of days for 1H 0323+342, PKS 1502+036 and PKS 2004-447. The minimum measured variability timescales in blazars can be as low as 200 seconds at very high energies ( $E > 200$  GeV) and 800 seconds at X-rays (see Aharonian et al. 2007, and references therein). At *Fermi*/LAT energies variability on scales of few hours has been detected in several blazars (e.g. Foschini et al. 2008; Tavecchio et al. 2010; Foschini et al. 2010a). In particular, the bright blazars 3C 454.3 and PKS 1510-089 showed variability on scales of 3–6 hours with flux  $\sim 10^{-5}$  ph cm $^{-2}$  s $^{-1}$  (Tavecchio et al. 2010), that is 1 – 2 orders of magnitude greater than the flux of the sources analyzed here. As discussed above, we expect to measure longer timescales on weaker sources, as a consequence of the longer time integration required to significantly detect the source. Our minimum timescale estimates are indeed approximately 1 – 2 orders of magnitude longer compared to those of the above-mentioned blazars. Therefore, we cannot exclude the possibility that variability in RL-NLS1 is as fast as the one observed in some of the most luminous blazars. The detection of shorter timescales on our sources is challenging due to their weakness. Ground-based Cherenkov telescopes may be more suited to search for shorter timescale variabilities, if the

spectrum of RL-NLS1 extend to very high energies. In principle variability can also be measured using the flux upper limits and the resulting minimum timescales would be below the results quoted in Table 1 (i.e. for PMN J0948+0022 we would obtain  $\tau \sim 1$  day). Upper limit of fluxes are however less reliable than direct flux measurement, since they depends on the contribution of nearby sources and of diffuse background.

The minimum  $e$ -folding timescale variability allow to estimate an upper limit for the size of the emitting region:  $R_{\text{blob}} \lesssim \delta c \tau / (1+z) \sim 0.5 - 6 \delta_1 \times 10^{17}$  cm, where  $\delta_1 = \delta/10$  is the relativistic Doppler factor and  $z$  is the redshift. With a jet aperture  $\theta_{-1} = \theta/0.1$  rad the distance at which most of the kinetic energy of the jet is dissipated and the  $\gamma$ -rays observed are produced (the so-called dissipation region), is  $R_{\text{diss}} \lesssim 0.2 - 2 \delta_1 / \theta_{-1}$  pc. The photon indices are rather steep ( $\Gamma < -2$ , with the only exception of the point at time  $\sim 75$  of PKS 2004-447), thus the inverse Compton peak lies below 100 MeV. In the framework of the blazar sequence (Fossati et al. 1998) the  $\gamma$ -ray emitting RL-NLS1 are therefore located in the region relevant to quasars. The photon index shows also some significant variations, e.g. at time  $\sim 750$  (MJD - 54682) the photon index of 1H 0323+342 underwent a  $6\sigma$  variation from  $\Gamma = -(2.46 \pm 0.06)$  to  $\Gamma = -(3.2 \pm 0.1)$  in 15 days (TS = 15 and 24, counts = 43 and 74 respectively). The corresponding photon flux is larger when the spectrum is steeper, so that the overall  $\gamma$ -ray luminosity does not change significantly. Another striking case is given at time  $\sim 550$  (MJD - 54682) of PKS 1502+036 for which the photon index shows a  $16\sigma$  variation from  $\Gamma = -(1.97 \pm 0.06)$  to  $\Gamma = -(4.7 \pm 0.2)$  in 15 days, although the TS values are much lower (10 and 11 respectively). Also in this case the overall  $\gamma$ -ray luminosity does not change significantly. This behaviour is in contradiction with the harder-when-brighter phenomenon observed in the X-ray spectra of several HBL (Brinkmann et al. 2005; Sembay et al. 2002) and at  $\gamma$ -ray energies of PMN J0948+0022 (Foschini et al. 2010c). This phenomenon is usually ascribed to the upshift of the inverse-Compton peak as the source brightens. The weakness of the sources prevents us from building a time-resolved detailed spectra and from drawing any conclusion about the eventual shift towards lower energies of the inverse-Compton peak in 1H 0323+342 and PKS 1502+036.

## 5 CONCLUSIONS

In this work, we report the discovery of a statistically significant variability in the  $\gamma$ -ray light curves of the four RL-NLS1 detected with *Fermi*/LAT, with minimum variability timescales in the range 3 – 30 days. This excludes a potential starburst origin of the  $\gamma$ -ray emission, and supports the hypothesis of the presence of a jet closely aligned to the line of sight. A hint for photon index variations on timescales  $\sim$ tens of days is also found in the data. Variability appears to be a feature common to the four first  $\gamma$ -ray detected RL-NLS1. The minimum timescales found in the *Fermi*/LAT energy range, appropriately scaled with the flux, are comparable to those found in the most luminous blazars. Thus, it is not possible to exclude variability as fast as that observed in blazars. This study goes in the same direction of the finding by Foschini et al. 2010c who reported compelling evidence

of similarities in the SED shape of PMN J0948+0022 (also analyzed here) and the archetypal blazar 3C 273. We are confident that in the near future more RL-NLS1 will be identified as  $\gamma$ -ray emitters among the many unidentified  $\gamma$ -ray sources observed by *Fermi*/LAT.

## REFERENCES

- Abdo A. A., et al., 2009a, ApJ, 699, 976  
 Abdo A. A., et al., 2009b, ApJ, 707, 727  
 Abdo A. A., et al., 2009c, ApJ, 707, L142  
 Abdo A. A., et al., 2010a, ApJ, 709, L152  
 Abdo A. A., et al., 2010b, ApJS, 188, 405  
 Aharonian F., et al., 2007, ApJ, 664, L71  
 Antón S., Browne I. W. A., Marchã M. J., 2008, A&A, 490, 583  
 Brinkmann W., Papadakis I. E., Raeth C., Mimica P., Haberl F., 2005, A&A, 443, 397  
 Decarli R., et al., 2008, MNRAS, 386, L15  
 Doi A., et al., 2006, PASJ, 58, 829  
 Drinkwater M. J., Webster R. L., Francis P. J., Condon J. J., Ellison S. L., Jauncey D. L., Lovell J., Peterson B. A., Savage A., 1997, MNRAS, 284, 85  
 Foschini L., Longo F., Iafrate G. et al., 2008, ATel 1784  
 Foschini L., et al., 2009, Advances in Space Research, 43, 889  
 Foschini L., et al., 2010a, MNRAS, 408, 448  
 Foschini L. for the Fermi/LAT Collaboration, Ghisellini G., Maraschi L., Tavecchio F., Angelakis E., 2010b, in “Accretion and ejection in AGN: a global view”, eds L. Maraschi, G. Ghisellini, R. Della Ceca & F. Tavecchio, Como (Italy), 22-26 June 2009, ASP Conference Series 427, p. 243  
 Foschini L., et al., 2010c, MNRAS submitted, [arXiv:1010.4434](https://arxiv.org/abs/1010.4434)  
 Fossati G., et al., 1998, MNRAS, 299, 433  
 Gaffney N. I., Lester D. F., Telesco C. M., 1993, ApJ, 407, L57  
 Gallo L. C., et al., 2006, MNRAS, 370, 245  
 Ghisellini G., Tavecchio F., 2009, MNRAS, 397, 985  
 Gu M., Chen Y., 2010, AJ, 139, 2612  
 Keel W. C., et al., 2006, AJ, 132, 2233  
 Kellermann K., et al., 1989, AJ, 98, 1195  
 Komossa S., et al., 2006, AJ, 132, 531  
 Marcha M. J. M., Browne I. W. A., Impey C. D., Smith P. S., 1996, MNRAS, 281, 425  
 Marconi A., et al., 2008, ApJ, 678, 693  
 Marscher A., 2009, In: “The Jet Paradigm - From Microquasars to Quasars”, ed T. Belloni, Lect. Notes Phys. 794, in press, ([arXiv:0909.2576](https://arxiv.org/abs/0909.2576))  
 Mattox J. R., et al., 1996, ApJ, 461, 396  
 Oshlack A. Y. K. N., Webster R. L., Whiting M. T., 2001, ApJ, 558, 578  
 Osterbrock D. E., Pogge R. W., 1985, ApJ, 297, 166  
 Pogge R. W., 2000, New Astronomy Review, 44, 381  
 Sembay S., Edelson R., Markowitz A., Griffiths R. G., Turner M. J. L., 2002, ApJ, 574, 634  
 Snellen I. A. G., McMahon R. G., Hook I. M., Browne I. W. A., 2002, MNRAS, 329, 700  
 Tavecchio F., et al., 2010, MNRAS, 405, L94  
 Williams R. J., Pogge R. W., Mathur S., 2002, AJ, 124, 3042

Yuan W., et al., 2008, ApJ, 685, 801  
Zhou H., et al., 2003, ApJ, 584, 147  
Zhou H., et al., 2007, ApJ, 658, L13

This paper has been typeset from a  $\text{\LaTeX}$  file prepared  
by the author.